ADVANCED FUNCTIONAL MATERIALS
www.afm-journal.de

Mass Transfer and Reaction Kinetic Enhanced Electrode for High-Performance Aqueous Flow Batteries

*Alolika Mukhopadhyay, Yang Yang, Yifan Li, Yong Chen, Hongyan Li, Avi Natan, Yuanyue Liu, Daxian Cao, and Hongli Zhu**

A scalable and efficient process to modify electrodes with enhanced mass transfer and reaction kinetics is critical for redox flow batteries (RFBs). For the first time, this work introduces electrochemical exfoliation as a surface modification method of graphite felt (GF) to enhance the mass transfer and reaction kinetics in RFBs. Anion intercalation and subsequent gas evolutions at room temperature for one minute expand the graphite layers that increase the electrode surface area. Meanwhile, sufficient oxygen functional groups are introduced to the electrode, resulting in enhanced reaction kinetics and improved hydrophilicity. Further, spin-polarized density functional theory is employed to reveal the role of oxygen functional groups in accelerating the vanadium redox reaction. Benefitting from sufficient oxygen groups, larger surface area, and superior wettability, the as-prepared exfoliated GF (E-GF) shows exceptional electrocatalytic activity with minimized overpotential, higher volumetric capacity, and improved energy efficiency. The redox flow battery assembled with the E-GF electrode delivers voltage and energy efficiencies of 89.72% and 86.41% at the current density of 100 mA cm^{-2}, respectively. Remarkably, compared to the traditional GF treatment method, the elimination of the high temperature and long-time treatment processes make this approach much more energy and time efficient, scalable, and affordable for large-scale manufacturing.

1. Introduction

Due to their abundance, solar and wind energy account for a significant share of renewables and are two of the most rapidly growing forms of renewable energy. However, challenges arise from their inherent intermittency and one approach to mitigate this discrepancy between the energy generation, and utilization is the integration of an energy storage system. Redox flow batteries (RFBs) are regarded as one of the most promising large-scale energy storage technologies. RFB's unique flow-based architecture allows the system to be scaled for specific applications with independent energy and power densities. One of the core components of the RFB stack is the electrode, which, to a certain extent, governs the overall performance of the RFB as the electrochemical reaction occurs at the electrode surface. In a flow battery, one of the most effective methods to reduce the stack size and the cost is to increase the operating current density, which also increases the power density and energy efficiency.[1] However, increasing the current density increases the voltage loss arising from the polarization that includes electrode kinetics, ohmic resistance, and mass transport limitations, leading to undesirable deterioration in the overall cell performance.[2] The ohmic resistance and the charge transfer polarization strongly depend on the physiochemical properties of the electrodes in the RFBs. The most commonly used electrodes in RFB are graphite felts (GFs) and carbon felts (CFs) by virtue of their high electrical conductivity, excellent stability, high corrosion resistance, and broad operational potential at a reasonable cost.[3] Despite the intensive research efforts, achieving high power density and energy efficiency are still a significant challenge for the RFB due to the hydrophobic nature of electrode arising from the high-temperature graphitization, poor catalytic activity contributing to higher polarization losses, and lack of abundant redox reaction sites owing to the low specific surface area.[4]

One effective way to enhance the electrocatalytic activity and thereby energy efficiency and power density is to deposit precious noble metals, such as Pt, Ru, Au, Bi, and Ir, but their high cost and higher hydrogen evolution rate hinder the large-scale commercialization.[5] Alternatively, low-cost metal oxides such as ZrO_2,[6] Mn_3O_4,[7] WO_3,[8] TiO_2,[9] CeO_2,[10] PbO_2,,[11] Ta_2O_5,[12] Nd_2O_3,[13] and Nb_2O_5[14] have also been deposited on the GF to enhance the electrocatalytic activity. However, several critical parameters like their nanosize, nonuniform distribution, structural stability in the harsh vanadium redox flow battery (VRFB) environment, and stability against dissolution severely

A. Mukhopadhyay, Dr. Y. Yang, Y. Chen, Dr. H. Li, A. Natan, D. Cao, Prof. H. Zhu
Department of Mechanical and Industrial Engineering
Northeastern University
360 Huntington Avenue, Boston, MA 02115, USA
E-mail: h.zhu@neu.edu
Y. Li, Prof. Y. Liu
Department of Mechanical Engineering
The University of Texas at Austin
110 Inner Campus Drive, Austin, TX 78705, USA
The ORCID identification number(s) for the author(s) of this article can be found under https://doi.org/10.1002/adfm.201903192.

DOI: 10.1002/adfm.201903192

reduce the activity of the metal oxide catalysts. Recently, nanocarbons such as graphene,[15] graphene oxide,[16] single-walled carbon nanotubes,[17] and multiwalled carbon nanotubes[18] were used to promote the electrochemical activity due to their unique physical and chemical properties facilitating high specific surface area and adequate reaction sites. However, the extensive utilization of graphene and carbon nanotube is not practical considering their high cost, the requirement of sacrificial metal, and rigorous reaction conditions. Other effective strategies like doping heteroatoms (nitrogen,[19] phosphate,[20] and boron[21]), surface modification to introduce carboxylic and hydroxyl groups,[22] activation in the CO_2 environment, wet etching using KOH to generate micropores,[23] and repeated NiO/Ni redox reaction to create graphenated graphite surface[24] have also been implemented to accelerate the reaction kinetics. Nonetheless, the requirement of high-temperature processing and tedious fabrication processes pose significant obstacles to cost-effective industrial scale application. Therefore, a low cost, facile, and scalable approach to introduce adequate functional groups, enhance the wettability, and specific surface area is desirable.

Herein, we propose a scalable approach to fabricate a unique hierarchical core–shell framework of graphite fibers by treating the GF using a controlled electrochemical exfoliation. The exfoliation was conducted in 0.1 M $(NH_4)_2SO_4$ solution by applying 10 V positive bias voltage. The obtained electrode after surface modification is rich in oxygen groups that 1) possesses a high specific surface area, 2) enhances the wettability leading to better electrolyte penetration and ion diffusion, 3) provides an adequate number of reaction sites, and 4) accelerates the charge and mass transportation by increasing the local charge concentration. Notably, the strong synergistic effect from high conductivity and the surface oxygen groups endow the E-GF electrode excellent electrochemical activity resulting in the high energy efficiency of 86.41% in the flow cell while operating at a high current density of 100 mA cm^{-2}. More importantly, due to the fast and room temperature modification of the E-GF electrode in aqueous solution, the entire process is fast, environmentally friendly, energy efficient, affordable, and scalable to the roll to roll large-scale manufacturing as a promising electrode treatment for various electrodes.

2. Results and Discussion

The exfoliation was carried out in a two electrode system in an aqueous solution containing 0.1 M $(NH_4)_2SO_4$ by applying a positive DC bias of 10 V to the GF anode (Figure S1, Supporting Information). At the first step of the exfoliation process, hydroxyl (OH•) and oxygen (O•) radicals are generated from the dissociation of water as the voltage applied surpasses the narrow electrochemical potential window of water splitting.[25] Initially, these radicals attack the graphite fibers, and oxidation or hydroxylation occurs at the edge sites and grain boundaries. As a result, the defective sites presented at the edge or grain boundaries open up,[26] which leads to depolarization and expansion of the graphite layers. The expanded graphite layers facilitate the intercalation of water (H_2O) molecules and sulfate anions (SO_4^{2-}) in between the layers, where the SO_4^{2-} reduces to sulfur dioxide (SO_2) and the H_2O molecule oxidizes to oxygen (O_2) causing gas evolution.[27] The produced gasses exert forces toward the much weaker van der Waals bonding between the layers triggering the exfoliation of the graphite fibers, as illustrated in **Figure 1**a. In addition to the oxidation of graphite, other reactions may also occur, including the evolution of CO_2, which also assists in the exfoliation of the graphite layers. As a result, a core–shell fiber morphology (Figure 1b) containing a solid core and a layered surface layer (shell), which increases the hydrophilicity and specific surface area, is formed. In addition, the unique hierarchical core–shell architecture contains abundant surface oxygen groups that simultaneously behave as the active sites for the redox reactions and promote charge and mass transportation, which are the critical requirements of an electrode for the RFB.

The surface modified E-GF sample, possessing a hierarchical core–shell architecture, can be directly used as the electrode in the VRFB and other aqueous RFB. As shown in Figure 1c, the flow battery performance can dramatically improve with the achieved structural complexity of the core–shell fiber framework, which facilitates electron and mass transportation leading to enhanced electrochemical performance. Remarkably, this approach of modifying the GF electrode can readily be scaled up for industrial-scale roll-to-roll manufacturing, as it only takes 1 min to exfoliate the GF. Accordingly, our strategy for the roll-to-roll exfoliation of GF to obtain super hydrophilic and electrocatalytically active E-GF electrode was schematically illustrated in Figure 1d.

Uniform and controlled exfoliation of the GF sample is crucial for obtaining a homogenous, well organized, and highly conductive core–shell configuration, as well as to prevent total disintegration of the GF structure and, therefore, maintain structural stability. **Figure 2**a illustrates the lab scale demonstration of the roll to roll set up for exfoliating a large piece of GF. In Figure 2b, it is apparent that the color of the surface modified E-GF sample transformed uniformly throughout its entire length of exfoliation, suggesting a homogenous treatment. Besides, after exfoliation, the GF retains its structural integrity and robustness, which verifies that the exfoliation occurs in a controlled manner. Further, to investigate the changes in wettability due to the exfoliation treatment, contact angles were measured for the pristine GF and E-GF, as shown in Figure 2c,d. The contact angle of pristine GF was measured to be 103°, whereas, it was difficult to measure the contact angle of E-GF as the water was absorbed by the felt instantaneously. In addition, pristine GF and E-GF electrodes were dipped into deionized water (Figure 2e), where the E-GF electrode sinks into the water, but the pristine GF floats at the top which further verifies the drastic improvement in the wettability of the E-GF. This indicates that the nature of the E-GF changed from hydrophobic to super hydrophilic due to the introduction of the surface oxygen groups. Similar results for the contact angle measurements were obtained when the exfoliation time was varied from 30 s to 4 min. The result implies that the E-GF contains sufficient oxygen groups due to the positive bias voltage making the felt super-hydrophilic. The excellent hydrophilicity will boost the electrolyte accessibility, accelerate the mass transfer, and reduce the charge transfer resistance

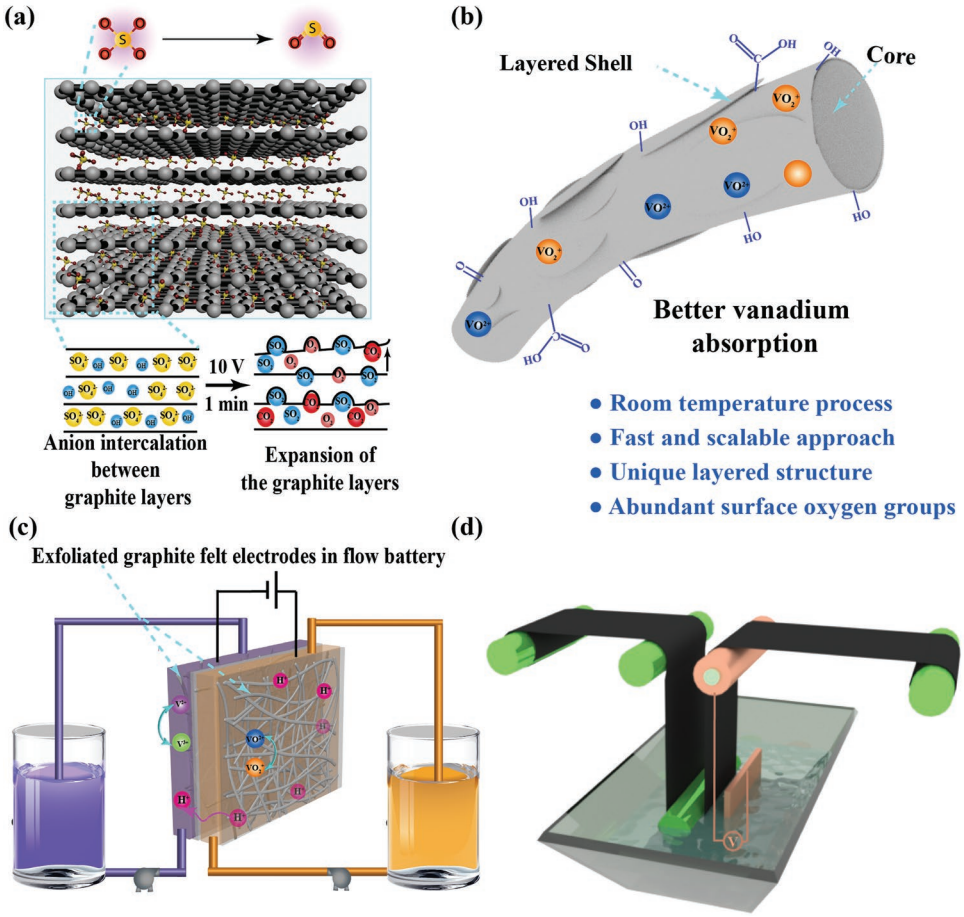

Figure 1. Schematic illustration of a) exfoliation mechanism showing the anion intercalation and subsequent reduction leading to expanded graphite layers. b) Core–shell fiber morphology showing the solid core and the exfoliated surface (shell). c) Application of the exfoliated GF electrode on both positive and negative sides in a redox flow battery. d) Schematic illustration of the large-scale roll to roll manufacturing of the exfoliated GF for industrial manufacturing.

of the electrode and increase the reversibility of the redox reactions.[28]

Further, the morphologies of the pristine GF and E-GF were investigated by scanning electron microscope (SEM) at different magnifications. Figure 2f depicts the SEM images of the surface of pristine GF at different magnifications showing a very smooth surface with very few defects and closely packed graphite layers. Arising from the expanded graphite at the outer surface, a well organized core–shell morphology with spaced and layered shell/surface is prominent in the SEM images of E-GF electrodes at different magnifications (Figure 2g). These changes in the morphology are due to the expansion of the edge and grain boundaries of the GF initiating expansion of the graphite layers. The expanded layers of graphite facilitate anion intercalation and consequently lead to a unique layered structure, which has a much larger specific surface area and promotes faster ion and electron transportation. The Brunauer–Emmett–Teller (BET) results show that the specific surface area of E-GF is 1.19 $m^2\ g^{-1}$, which is two times larger than that of the pristine graphite felt (0.55 $m^2\ g^{-1}$) (Figure S2, Supporting Information). The enlarged specific surface area of the E-GF, compared to the tightly packed pristine GF, benefits the electrochemical activity of the vanadium redox couples by increasing the number of active sites on the surface.

To optimize the exfoliation process, a systematic study was conducted where the constant bias voltage was applied to the GF electrodes for different time periods (30 s to 4 min). The variation in cyclic voltammetry (CV) curves for positive (VO_2^+/VO^{2+}) and negative (V^{3+}/V^2) electrolytes were examined for the various exfoliation times. Several critical parameters such as the redox onset potential, peak potential separation (ΔE), and the ratio of the peak cathodic (I_{Pc}) and anodic (I_{Pa}) currents were evaluated in a three-electrode system to fundamentally understand the electrocatalytic activity of different E-GF electrodes for VO_2^+/VO^{2+} and V^{3+}/V^{2+} redox couples. The E-GF electrode exfoliated for 1 min shows the optimal redox onset potentials, lowest ΔE, and highest $-I_{Pc}/I_{Pa}$ ratio, suggesting that the exfoliation time of 1 min provides the best performance compared to the exfoliation time of 30 s, 2 min, 3 min, and 4 min (Figure S3a, Supporting Information). The optimum performance of the 1 min E-GF electrode is because a considerable amount of graphite flakes were exfoliated and released into the electrolyte solution when the exfoliation time was increased beyond 1 min, as shown in Video S1 (Supporting Information). Also, the edge of the graphite expands

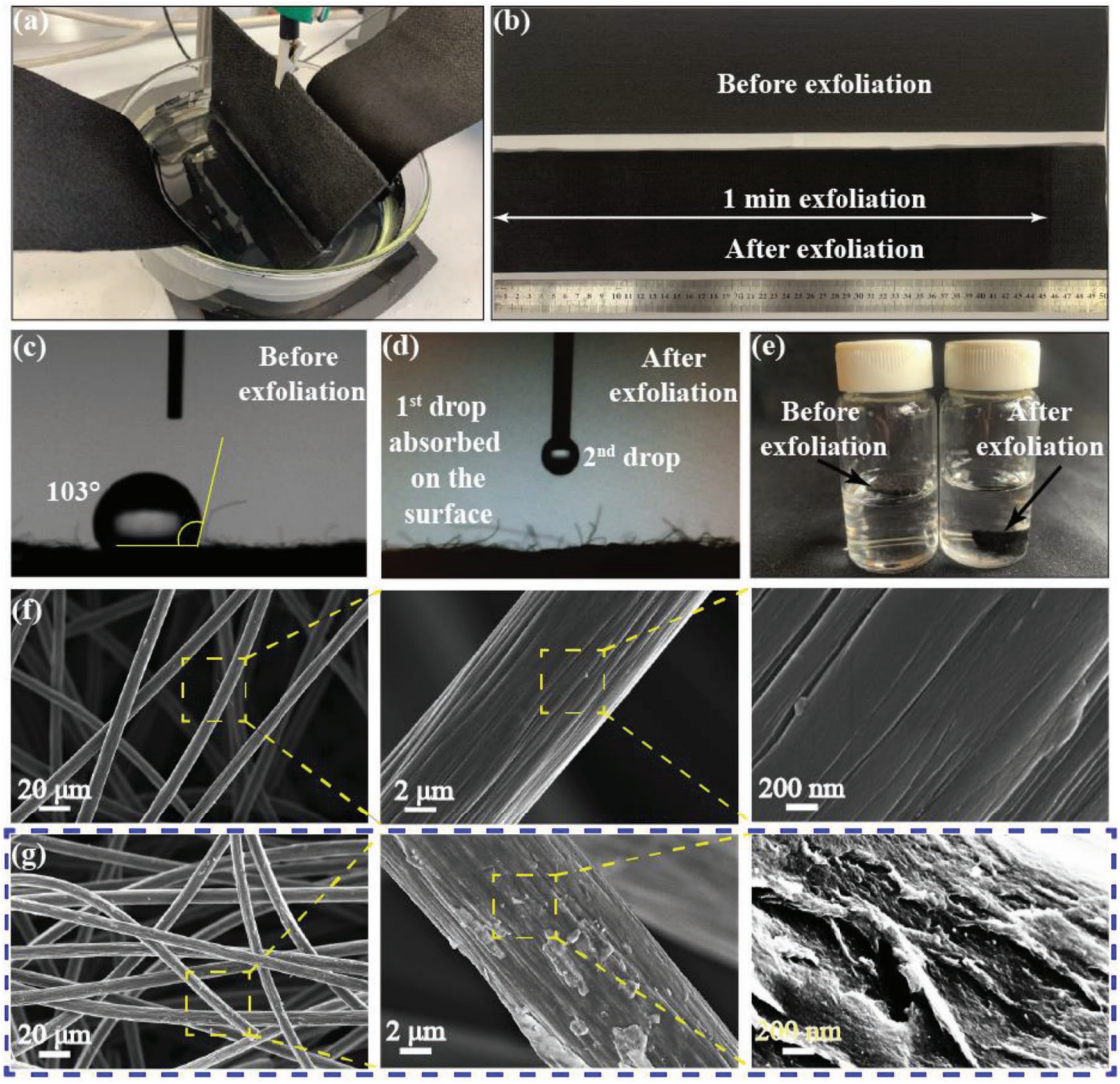

Figure 2. Digital photographs of a) Roll to roll exfoliation set up in lab scale, b) GF before and after exfoliation. Contact angle measurement of c) pristine GF and d) E-GF electrode. e) Digital photographs of pristine GF and E-GF electrode highlighting the wettability of E-GF compared to the pristine GF in deionized water. SEM images of f) pristine GF and g) E-GF at different magnifications of 1000 X, 5000 X, and 50 KX.

ten times than its initial state after 1 min due to the vigorous gas evolution leading to excessive swelling of the graphitic layers.[27]

Moreover, in addition to the $(NH_4)_2SO_4$ solution, various aqueous electrolyte solutions including 0.1 M $(NH_4)_2SO_4$ with (2,2,6,6-tetramethylpiperidin-1-yl)oxyl (TEMPO), 0.1 M $(NH_4)_2SO_4$ with 10% ethanol, 0.1 M $(NH_4)_2SO_4$ with 0.1 M sodium hydroxide (NaOH), and 0.1 M sulfuric acid (H_2SO_4) were used to prepare 1 min E-GF electrodes and their CV curves were examined. The 0.1 M $(NH_4)_2SO_4$ electrolyte exhibited the best performance (Figure S3b, Supporting Information) among the others. Thus, the CV curves of the E-GF electrodes prepared by applying a positive 10 V DC voltage to the GF anode in 0.1 M $(NH_4)_2SO_4$ aqueous solution for 1 min were used to compare with the pristine GF and other commonly used modifications of electrodes such as acid treated GF (A-GF) and thermally treated GF (T-GF).

Further, the CV curves (**Figure 3**) of the various GF electrodes are evidence of substantial enhancement in the electrochemical properties of the as-prepared E-GF compared to the pristine GF, A-GF, and T-GF. In the CV curves of positive electrolyte (VO_2^+/VO^{2+} redox couples), as depicted in Figure 3a, the E-GF electrode exhibited significantly better redox onset potentials, a ΔE of 124 mV and $-I_{Pc}/I_{Pa}$ ratio of 0.86; while the pristine GF, A-GF, and T-GF displayed ΔE of 139, 149, and 130 mV and $-I_{Pc}/I_{Pa}$ ratios of 1.05, 0.47, and 0.60, respectively. More importantly, the E-GF electrode displayed a more striking effect of accelerating the sluggish kinetics of V^{3+}/V^{2+} redox couple. This was demonstrated by clearly defined redox peaks with better redox onset potentials (the potential at which the reduction is started),[29] a ΔE of 160 mV, and a $-I_{Pc}/I_{Pa}$ ratio of 1.44. Furthermore, no defined redox peaks were obtained for the pristine GF and A-GF (Figure 3b) for the V^{3+}/V^{2+} redox couple. In addition, significant undesirable hydrogen evolution reaction

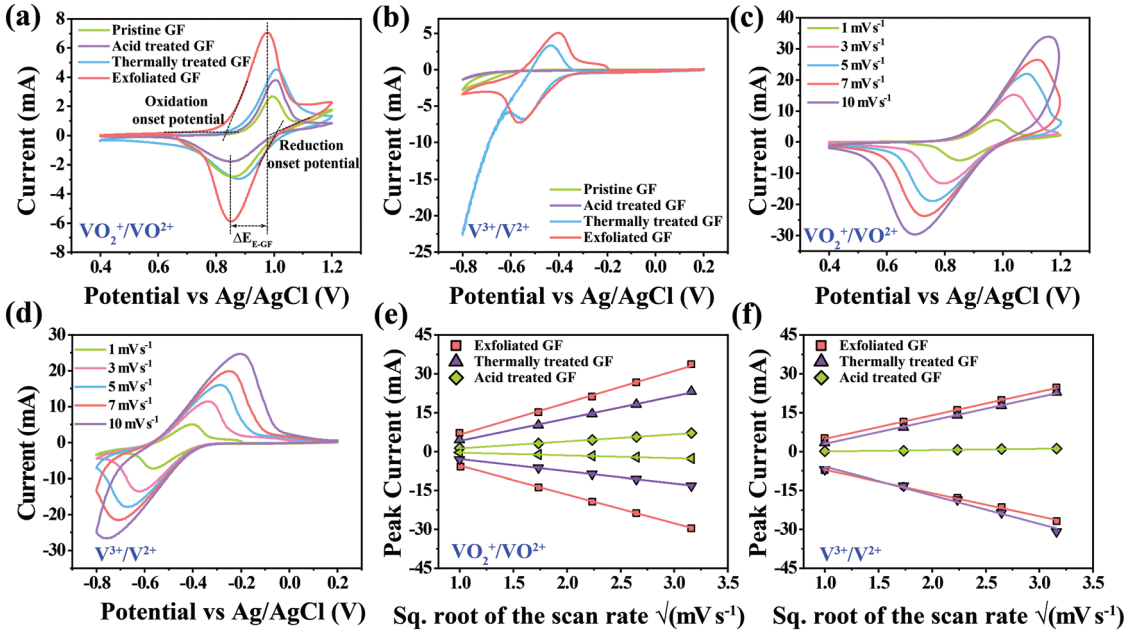

Figure 3. Electrochemical analysis of the prepared E-GF electrode (exfoliated for 1 min) compared to pristine GF, A-GF, and T-GF in 0.1 M $VOSO_4$ in 3 M H_2SO_4. CV curves of E-GF electrode compared to the pristine GF, A-GF, and T-GF for a) VO_2^+/VO^{2+} and b) V^{3+}/V^{2+} redox couples at 1 mV s^{-1} scan rate. CV curves of E-GF electrode at various scan rates ranging from 1 to 10 mV s^{-1} for c) VO_2^+/VO^{2+} and d) V^{3+}/V^{2+} redox couples. The plot of anodic (I_{Pa}) and cathodic (I_{Pc}) peak currents of E-GF electrodes versus the square root of the scan rates for e) VO_2^+/VO^{2+} and f) V^{3+}/V^{2+} redox couples.

(HER) was observed within the working potential window on the T-GF electrode, which will eventually cause capacity fade in the flow cell.

The superior electrochemical performance of E-GF electrode toward positive (VO_2^+/VO^{2+}) and negative (V^{3+}/V^{2+}) electrolytes is an indication of more rapid and reversible redox reactions with minimized overpotential, which can be ascribed to the well organized hierarchical core–shell configuration containing massive surface oxygen groups. The incorporated oxygen groups behave as active sites for the redox reaction resulting in enhanced kinetics at the electrode-electrolyte interface, faster charge and mass transportation, and improved wettability enabling better electrolyte accessibility. To further investigate the reaction kinetics and evaluate the mass transfer behavior, the CV curves of the E-GF electrodes were also acquired at different scan rates ranging from 1 to 10 mV s^{-1} for VO_2^+/VO^{2+} and V^{3+}/V^{2+} redox couples, as displayed in Figure 3c,d, respectively. The CV curves of T-GF (Figure S4a, Supporting Information) and A-GF (Figure S4b, Supporting Information) electrodes were also obtained at various scan rates for VO_2^+/VO^{2+} redox couple. In addition, the peak current densities of VO_2^+/VO^{2+} (Figure 3e) and V^{3+}/V^{2+} (Figure 3f) redox couples were plotted as a function of the square root of the scan rates, which exhibit linear shape and imply a diffusion-controlled reaction. Moreover, the slopes of the E-GF electrode, corresponding to the reduction and oxidation of VO_2^+/VO^{2+} and V^{3+}/V^{2+} redox couples are the highest among the pristine GF and A-GF (Figure S4c, Supporting Information), indicating a distinct improvement in the mass transfer kinetics according to the Randles-Sevcik equation (Equation S1, Supporting Information). This substantial enhancement in diffusion is due to the superhydrophilic nature of the E-GF, which is achieved by the introduction of the oxygen functional groups that are extremely beneficial for the performance of the flow cell.

To get further insight into the elemental composition and presence of surface oxygen groups in the E-GF electrode, X-ray photoelectron spectroscopy (XPS) was conducted. Only 3.66% atomic oxygen content was detected in the pristine GF sample (attributed to the spontaneous adsorption of oxygen on the carbon surface in the air), while 25.48% atomic oxygen content was detected in the E-GF sample. This can be attributed to the oxidation of the E-GF sample due to the application of positive DC voltage during exfoliation. Thus, the oxygen to carbon ratio was increased from 0.039 (pristine GF) to 0.361, which confirms the grafting of different oxygen functional groups on E-GF. For further analysis, the pristine GF and E-GF's high-resolution spectra of the C1s region, presented in **Figure 4**a, were deconvoluted into four peaks at binding energies of 284.6, 285.8, 286.9, and 288.8 eV each representing different carbon bonds. The peak at 284.6 eV is associated with the core level carbon atoms (C=C/C−C) in the graphitic carbon, whereas, the peaks at 285.8, 286.9, and 288.8 eV were assigned to the hydroxyl (−C−O−),[30] ester (−COO−)/carbonyl (−C=O),[31] and carboxyl (−O−C=O)[32] functional groups, respectively. Another peak at 290.5 eV was also present in both of the electrodes attributable to the π to π^* shake up satellite contributions.[33] The intensities of all peaks related to the oxygen functional groups were increased in the E-GF electrode compared to the pristine GF electrode, implying the incorporation of oxygen groups in the E-GF electrode. Since the oxygen functional groups are related to the active sites for the vanadium ions, the high-resolution O1s spectra of pristine GF and E-GF were also fitted by deconvoluting three peaks at binding energies of 532.9, 533.1, and 531.8 eV, corresponding to the

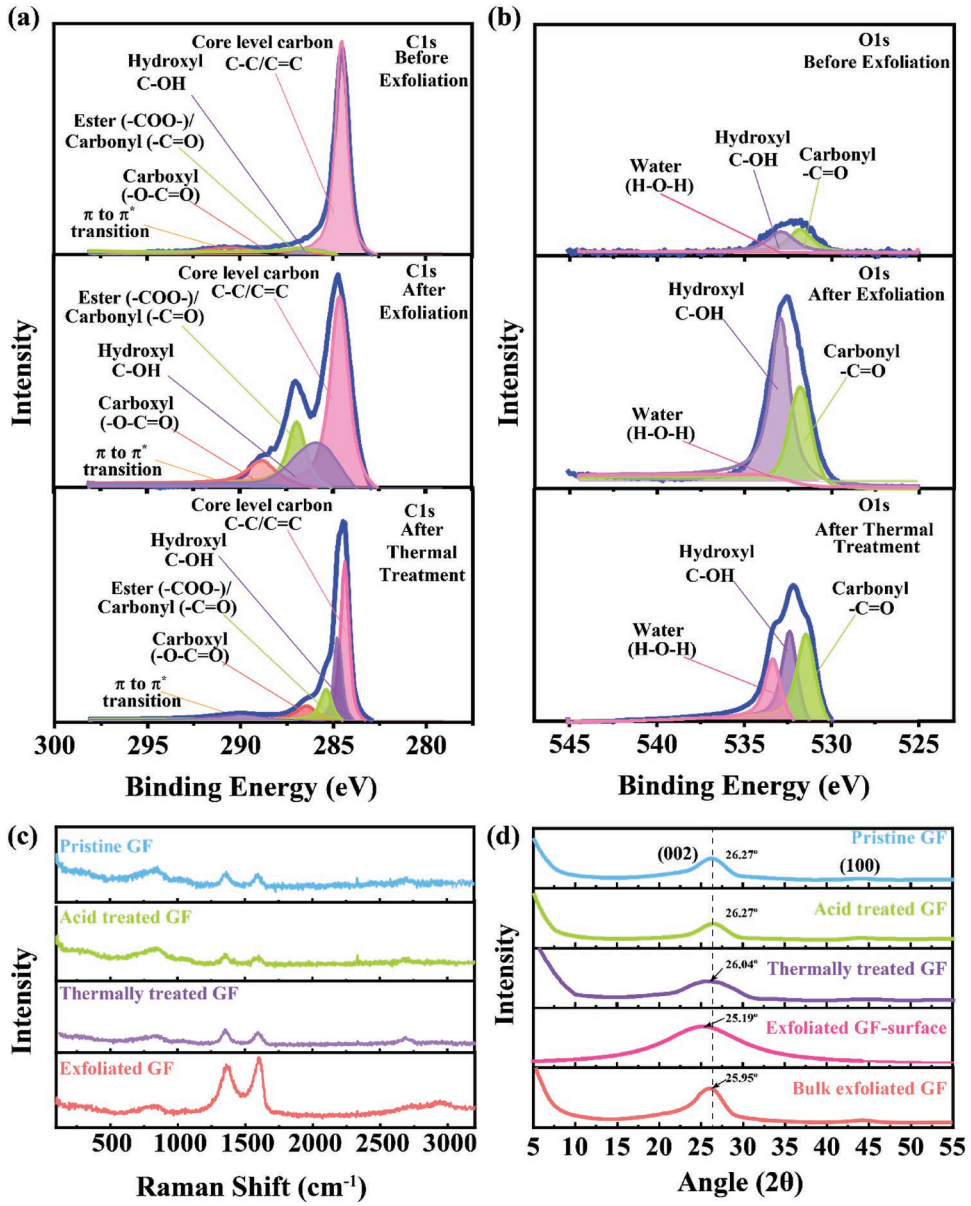

Figure 4. High-resolution XPS spectra of pristine, exfoliated, thermally treated graphite felts for a) C1s b) O1s. c) Raman spectra and d) XRD spectra for pristine, acid treated, thermally treated, and exfoliated graphite felt.

hydroxyl (−OH), water (H−O−H), and carbonyl (−C=O), respectively.[32,34] In E-GF electrode, the intensity of the −OH groups is greater than that of the −C=O, indicating that the exfoliation benefits the formation of −OH groups. These −OH groups arise from the broken C=C bonds due to the strong oxidation and part of the −OH groups further oxidize and convert to −C=O.[35] It is worth mentioning that the −OH groups offer more electrochemically active sites compared to any other functional groups and thereby best facilitate the redox reaction of vanadium.[36] Additionally, the −OH and −C=O groups on the surface of the E-GF electrode enhance its hydrophilicity, which assists the electrolyte and ion diffusion through the E-GF electrode. However, the role of the oxygen functional groups in the electroactivity of the carbonaceous electrodes in enhancing the kinetics of the vanadium redox couples is still contested. In the early work of Skyllas-Kazacos and Sun,[22] they claimed that the surface active functional groups C−O and C=O, added by thermal treatment of the carbon felt, was beneficial for the VO_2^+/VO^{2+} redox couple. In addition, Noack et al. confirmed that the number of hydroxyl groups correlates to the kinetics of the VO_2^+/VO^{2+} redox couple and is indeed beneficial, while no such correlation was found for the V^{2+}/V^{3+} redox couple.[37] Conversely, according to Fink et al. the redox reaction trends for V^{2+}/V^{3+} and VO_2^+/VO^{2+} redox couples are always diametrical. Therefore, the −OH, −C=O, and −O−C=O groups accelerate the reaction rate for V^{2+}/V^{3+}, but decrease the reaction rate for the VO_2^+/VO^{2+} redox couple, whereas, the graphitic carbon exhibits the reverse trend.[38] Besides, Bourke et al. observed

that the rate constants for the VO^{2+}/VO_2^+ redox couple are higher than the V^{2+}/V^{3+} redox couple except when the oxygen functional groups are incorporated into the electrode by anodization, explaining the contradictory results in the literature.[39] Therefore, further in-depth studies are necessary to understand the effect of exfoliation on the kinetics of the vanadium reactions. Furthermore, wide range XPS scans obtained for E-GF electrode, as illustrated in Figure S6 (Supporting Information), exhibit two new peaks for N1s (401.8 eV) and S2p (168.8 eV) compared to the pristine GF, which was also evident in the high-resolution scans for N1s and S2p (Figure S7, Supporting Information). The presence of N1s and S2p peaks are associated with the residual ammonia and sulfate ions due to the use of $(NH_4)_2SO_4$ electrolyte solution in the exfoliation process.

Moreover, as illustrated in Figure 4c, Raman spectra were also used to investigate the structural disorder of the GF before and after exfoliation. The Raman spectra for the GF samples exhibited two prominent bands one at 1355 cm^{-1} (D band) corresponding to the breathing mode of the sp^2 carbon atoms activated by the presence of defects or structural disorder and another at 1591 cm^{-1} (G band) associated with the well ordered sp^2 domains.[6,40] Intensity ratio of the D band and G band (I_D/I_G) indicates the existence of the defects. The pristine GF exhibited an I_D/I_G ratio of ≈1.13, which further increases for the A-GF (1.29) and T-GF (1.17) and diminished to ≈0.87 for the E-GF, verifying that the E-GF has lesser defect density compared to the pristine GF, A-GF, and T-GF. Hence, it is evident that the crystalline structure of the GF was not affected by 1 min exfoliation and thus, can maintain its high conductivity after 1 min exfoliation. The ability to maintain crystalline structure was also verified by the X-ray diffraction pattern (XRD) of the E-GF compared to the pristine GF, A-GF, and T-GF, as demonstrated in Figure 4d. All the samples exhibit the most significant diffraction peak at around ≈26.3° with little deviation corresponding to the (002) plane indicating highly organized crystal structure with an interlayer spacing of ≈0.338 nm[16] and weak diffraction peaks around 44.3° associated with the (100) plane. It is worth mentioning that no visible changes in the layer distance between the pristine GF and the E-GF samples were observed since the expansion occurs only at the outer surface. However, the solid core dominates the XRD results suppressing the small changes in peak positions originating from the layered shell due to the expanded graphite layers. However, the XRD spectra of the shell (the scraped off surface) of E-GF electrode exhibits the main peak at 25.19° verifying the expansion of graphite layers at the outer surface forming a well-organized core–shell structure. This structure accelerates the charge and mass transportation leading to better electrochemical performance.

To further investigate the electrochemical activity of the E-GF electrodes with different exfoliation times, electrochemical impedance spectroscopy (EIS) was carried out at open circuit potential and the associated Nyquist plots are demonstrated in **Figure 5**a. All the Nyquist plots exhibit a semicircle at high frequency due to the charge transfer process and a linear region at the low frequency due to the diffusion of the vanadium ions through the solution, indicating that the reaction is governed by both charge transfer and diffusion.[41] From the fitted curves, as illustrated in Figure S8 (Supporting Information), the 30 s, 1 min, and 2 min exfoliated samples displayed ohmic resistance (R_s) of 0.111, 0.110, and 0.124 Ω and charge transfer resistance (R_{ct}) of ≈0.438, 0.391, and 0.294 Ω, respectively. Hence, it can be concluded that the variation in exfoliation time has a negligible effect on R_s, which is the ohmic resistance of the cell. However, the R_{ct} exhibits an inverse trend with increasing exfoliation time. The relationship indicates an acceleration of the charge transfer between the vanadium ions and the electrodes, attributable to the increase in the concentration of surface oxygen groups. This is caused by the overoxidation of the E-GF electrodes from longer exfoliation times.

Conversely, the area specific resistance (ASR) that combines the charge transfer, ohmic, and mass transport resistance of the flow cell seems to be lowest for 1 min E-GF electrode compared to the 30 s and 2 min E-GF electrodes, as shown in Figure 5b. The ASR values are 3.11, 2.33, and 4.45 Ω cm^2 during charge and 4.61, 2.65, 7.81 Ω cm^2 during discharge for 30 s, 1 min, and 2 min E-GF, correspondingly, which undoubtedly endorse the superiority of the 1 min E-GF electrode. In addition, the voltage profiles of the 1 min E-GF electrode has 3 and 14 mV less overpotential (Figure 5c) at the same current density of 40 mA cm^{-2} compared to the 30 s and 2 min E-GF electrodes during the charge and discharge of the flow cell, respectively. The lower overpotential indicates higher electrochemical activity of the 1 min E-GF electrode. The performance of the 30 s, 1 min, and 2 min E-GF was also analyzed based on the coulombic efficiency (CE), voltage efficiency (VE), and energy efficiency (EE) at current densities ranging from 40 to 200 mA cm^{-2}, as demonstrated in Figure 5d–f. The CE of all the E-GF electrodes were similar at each current density, whereas, the VE and EE of the 1 min E-GF electrode were much higher than the 30 s and 2 min E-GF electrodes at all the current densities.

The enhancement in the electrochemical properties of the 1 min E-GF electrode is more predominant at a higher current density of 200 mA cm^{-2}, where the 1 min E-GF electrode achieves a high capacity but the 2 min E-GF electrode can not complete charge–discharge cycles within the same operating voltage window. The 1 min E-GF electrode acquired capacities of 23.94, 22.56, 21.45, 19.89, 16.66, and 8.18 Ah L^{-1} at the current densities of 40, 60, 80, 100, 150, and 200 mA cm^{-2}, respectively, whereas the 30 s electrode acquired capacities of 18.76, 17.71, 16.66, 15.62, 14.28, and 8.14 Ah L^{-1} at the current densities of 40, 60, 80, 100, 150, and 200 mA cm^{-2}, respectively, and 2 min E-GF electrode can run a maximum current density of 100 mA cm^{-2} (Figure 5g). In addition, the 30 s, 1 min, and 2 min E-GF electrodes regain ≈88%, 98%, and 68% of their original capacity when returned to the initial current density of 40 mA cm^{-2}, which further confirms the superior rate performance of 1 min E-GF electrode due to the higher electrical conductivity of the 1 min E-GF electrode among the others (Figure S9, Table S2, Supporting Information). We believe that the 1 min E-GF electrode preserves an optimum balance between the conductivity, surface area, and wettability since the conductivity decreases with an increase in exfoliation time (Table S2, Supporting Information) that negatively influences the performance of the electrode. This behavior is also consistent with the study reported on the electrochemical oxidation of graphite felt electrode by Cao et al.,[33] where they

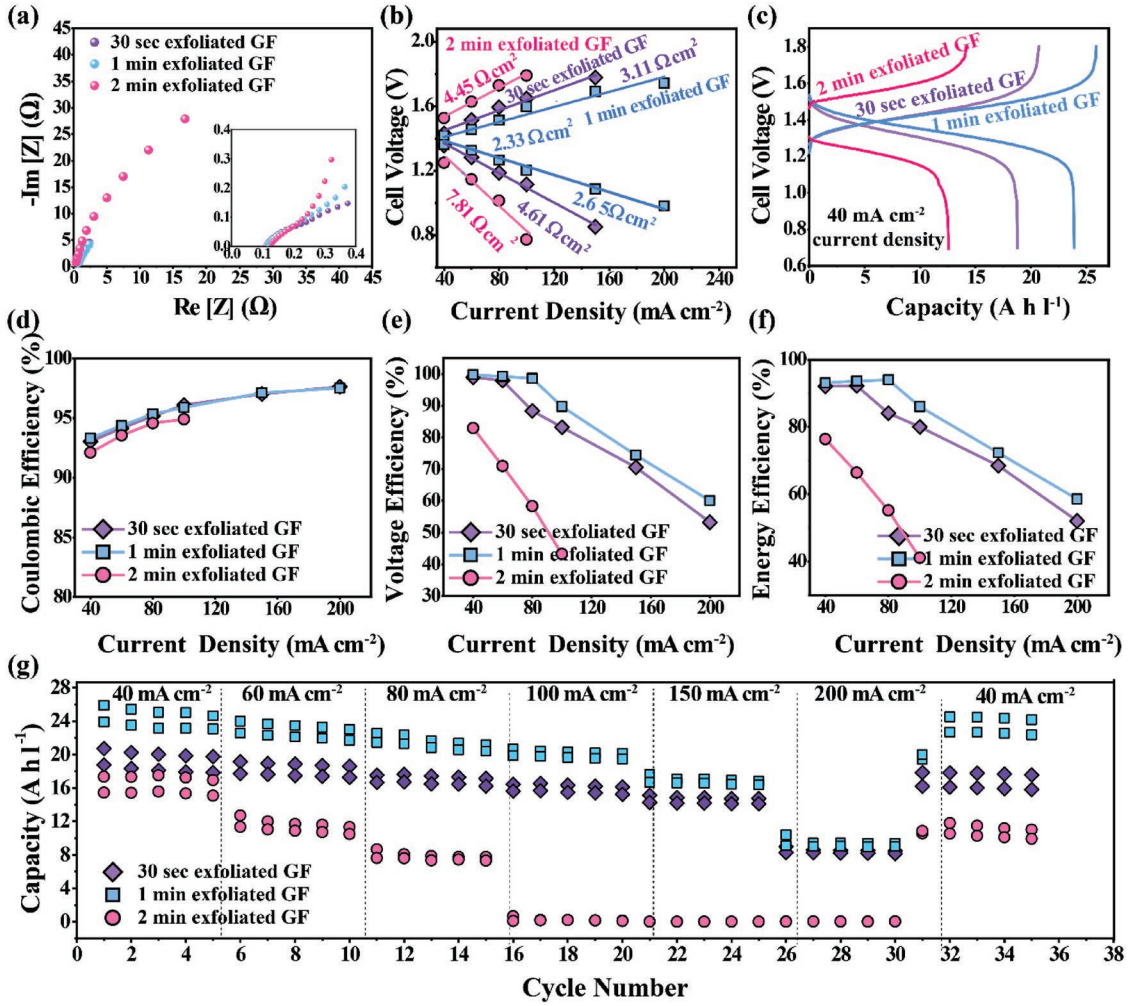

Figure 5. Electrochemical performance of VRFB employing E-GF electrodes exfoliated for 30 s, 1 min, and 2 min. a) Nyquist plots of E-GF electrodes treated for 30 s, 1 min, and 2 min. b) Fitted polarization curves highlighting the slopes of the curves for charge and discharge that represent the ASR. c) Charge–discharge profiles of E-GF electrodes at 40 mA cm^{-2}. d) Coulombic efficiency, e) voltage efficiency, and f) energy efficiency of E-GF electrodes at current densities of 40, 60, 80, 100, 150, and 200 mA cm^{-2}. g) Rate performance of E-GF electrodes at current densities of 40, 60, 80, 100, 150, and 200 mA cm^{-2}.

concluded that the kinetics of the vanadium redox reactions are always dependent on two competing factors, the amount of incorporated oxygen groups and surface area of the electrode. Simultaneously, the E-GF electrode becomes more hydrophilic as the exfoliation time increases, facilitating better electrolyte accessibility. Accordingly, the 1 min was chosen as the optimal exfoliation time and is used for further experiments.

To further confirm the electrochemical performance, EIS for all the control samples with different treatment types were conducted in the flow cell (**Figure 6**a and Figure S10, Supporting Information). The pristine GF, A-GF, T-GF (treated for 10 h), and E-GF electrodes exhibit an R_s of 0.128, 0.103, 0.105, and 0.101 Ω and R_{ct} of 10.36, 4.09, 0.39, and 0.36 Ω. The R_{ct} gradually decreases in the order of pristine GF, A-GF, T-GF, and E-GF, indicating excellent charge transfer capability of the E-GF electrodes due to the improved hydrophilicity. Furthermore, ASR obtained for the A-GF, T-GF, and E-GF electrodes are 10.60, 4.81, and 2.33 Ω cm^2 during charge and 16.45, 7.50, 2.65 Ω cm^2 during discharge (Figure 6b), suggesting the lowest ASR for the E-GF electrode among the others. Figure 6c exhibits the charge–discharge voltage profiles at the same current density, where a noticeably reduced overpotential of 470 and 579 mV compared to pristine GF, 250 and 290 mV compared to A-GF, and 180 and 160 mV compared to T-GF was achieved during charge and discharge, respectively. The E-GF electrode attains a capacity of 23.94 A h L^{-1}, while the T-GF, A-GF, and pristine GF electrodes obtain 22.48, 14.9, and 7.4 A h L^{-1} respectively, at the same current density (40 mA cm^{-2}) and operating voltage window. The obtained results suggest the effect of exfoliation of the GF electrode leads to smaller overpotential and a significantly higher capacity than the pristine GF, which can be ascribed to the abundant active reaction sites, larger surface area, and enhanced wettability allowing the rapid mass transfer. It is worth mentioning that the E-GF electrode exhibited a predominant mass transfer limited region toward the end of the charge/discharge curves, which is related to "electrode starvation" as mentioned by Zawodzinski et al.[42] "Electrode starvation" arises when all the electroactive species

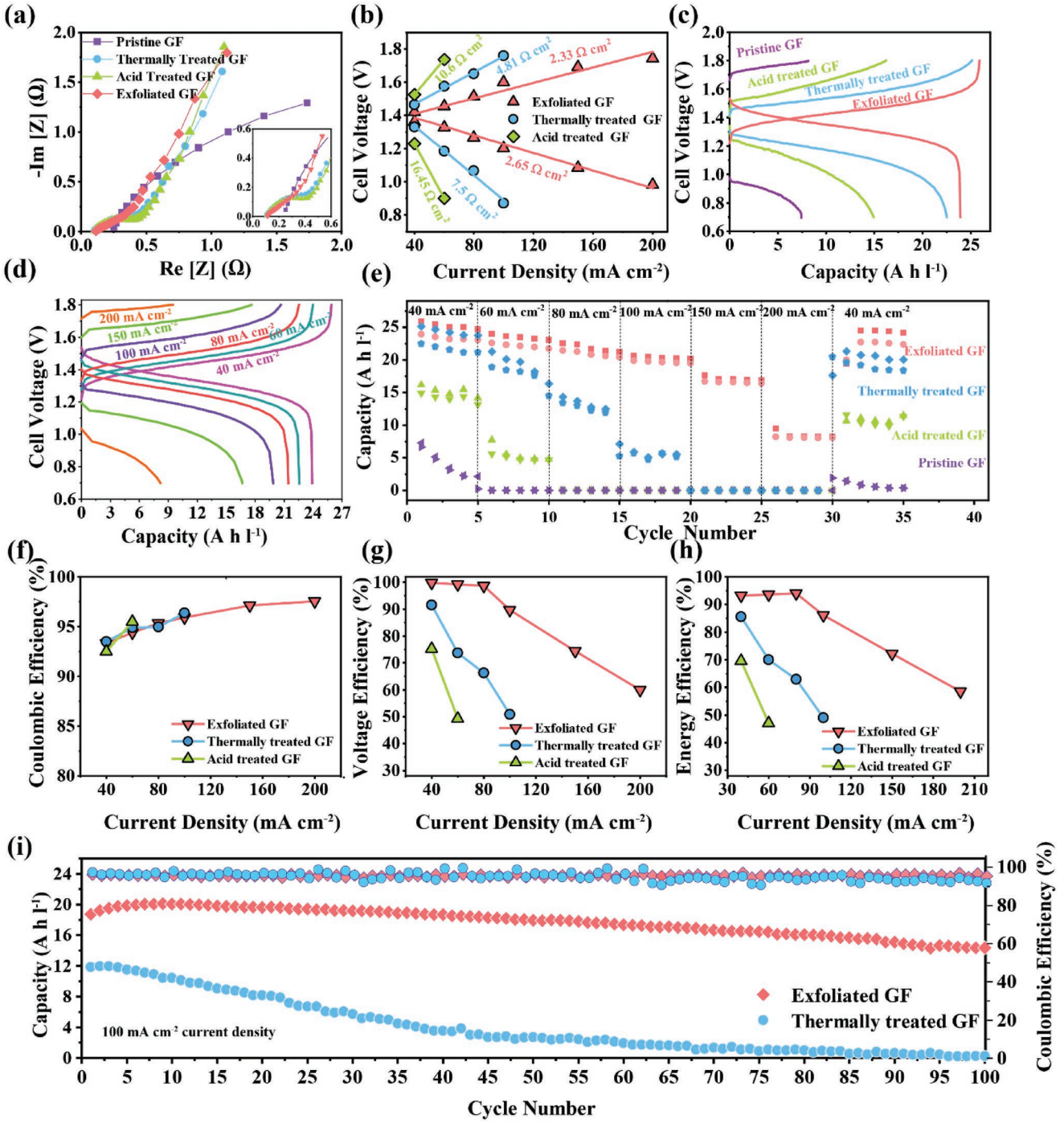

Figure 6. Electrochemical performance of VRFB employing pristine GF, A-GF, T-GF, and E-GF electrodes. a) Nyquist plots of pristine GF, A-GF, T-GF, and E-GF electrodes. b) Fitted polarization curves of pristine GF, A-GF, T-GF, and E-GF electrodes. c) Charge–discharge profiles of pristine GF, A-GF, T-GF, and E-GF electrodes at 40 mA cm^{-2}. d) Charge–discharge profiles of E-GF electrodes at current densities of 40, 60, 80, 100, 150, and 200 mA cm^{-2}. e) Rate performance of pristine GF, A-GF, T-GF, and E-GF electrodes at different current densities of 40, 60, 80, 100, 150, and 200 mA cm^{-2}. f) CE, g) VE, and h) EE of A-GF, T-GF, and E-GF electrodes at different current densities (40, 60, 80, 100, 150, and 200 mA cm^{-2}). i) Cycling stability representing the discharge capacity and CE of E-GF electrode compared to T-GF electrode for 100 continuous charge–discharge cycling at 100 mA cm^{-2}.

completely converts at the operating current density causing a mass transport limited region in the charge–discharge curves. Therefore, the presence of "electrode starvation" along with the higher capacities for the E-GF electrode further indicate better utilization of the electrolyte compared to the other samples at the same current density.

Likewise, the smaller overpotential is also well defined in the charge–discharge profiles of the E-GF electrodes at different

current densities (Figure 6d), where the voltage gap rises with the increase in the current density leading to a reduction in achieved capacity with the increasing current density due to the increased ohmic loss and mass transport limitations at higher current densities. As depicted in Figure 6e, the E-GF electrode regains ≈98% of its initial capacity when returned to the initial current density, evidence of a much-enhanced rate performance of E-GF electrode even at higher current densities compared to the pristine GF, A-GF, and T-GF. The rate performance (Figure S11, Supporting Information) and voltage profiles (Figure S12, Supporting Information) of 30 h thermally treated electrode are also compared with the performance of E-GF electrode and 10 h treated T-GF electrode, where the E-GF showed much better performance at high current densities compared to the others. The drastic improvement in the rate performance can be attributed to the rapid electron transportation and super hydrophilic nature of the E-GF electrode caused by the functional oxygen groups.

Notably, except the E-GF, all other electrodes illustrated substantially high overpotential for charge and discharge at a high current density and cannot successfully run within the operating voltage window. Consequently, the efficiencies for pristine GF were excluded from Figure 6f–h, while for A-GF and T-GF they were obtained by varying the current density from 40–60 and 40–100 mA cm^{-2}, and for E-GF the current density was varied from 40–200 mA cm^{-2}. As anticipated, different modifications have a negligible effect on the CE at the same charge–discharge rate, and the CE increases with an increase in the current density owing to the lower self-discharge across the membrane in the shorter cycle time with the increasing current density.[43] However, the modifications significantly impact the VE of the cell, which are 99.81, 99.23, 98.63, 89.72, 74.38, and 60.95% for E-GF at current densities of 40, 60, 80, 100, 150, and 200 mA cm^{-2}, respectively. The VE for T-GF was 91.43, 73.71, 66.25, and 50.85% at current densities of 40, 60, 80, and 100 mA cm^{-2}, respectively. Lastly, the VE for A-GF was 75.23 and 47.14% at current densities of 40 and 60 mA cm^{-2}, respectively. Meanwhile, the E-GF attains EE of 93.13, 93.62, 92.04, 86.41, 72.24, and 58.51% at current densities of 40, 60, 80, 100, 150, and 200 mA cm^{-2}, respectively. The achieved VE and EE for E-GF at all current densities are clear indications of the improved electrocatalytic effect and rapid charge transfer of the E-GF electrode accredited to the introduction of sufficient surface oxygen groups without sacrificing the high electrical conductivity and extreme hydrophilicity prompting instantaneous absorption of the electrolytes onto the E-GF surface.

Further, to verify the electrochemical reversibility and stability, a constant current charge–discharge cycling of the E-GF and T-GF electrode was conducted at a current density of 100 mA cm^{-2}, as demonstrated in Figure 6i, where the E-GF electrode displays a stable CE of ≈96% throughout the cycling. Although, both the electrodes showed a gradual capacity fade due to the vanadium crossover across the Nafion membrane,[44] the capacity retention of the E-GF electrode is much higher compared to the T-GF electrode. Faster capacity fade of the T-GF electrode can be attributed to the much higher overpotential compared to the E-GF electrode at the operating current density. The capacity at the first cycle for E-GF electrode is 18.84 A h L^{-1}. After 100 cycles, the capacity maintains at 14.43 A h L^{-1}, which shows an average capacity fade of 0.23% per cycle, proving the enhanced stability of the E-GF compared to the T-GF.

Thus, the obtained results validate the superior electrocatalytic activity and stability of the E-GF electrode compared to the pristine GF, A-GF, and T-GF electrode in the VRFB. The surface oxygen groups catalyze the VO_2^+/VO^{2+} reaction due to two main reasons. The first is that the C—O groups intensify the adsorption of the VO^{2+} ions by supplying protons that facilitate the transport of the mass from the solution to the electrode surface. The second reason is that the charge and discharge process at the positive side requires the transfer of an oxygen atom along with the electron transfer and the existence of the C—OH and O—C=O groups on the GF surface assists in the oxygen transfer,[42] which is a rate-determining step in the VRFB.

To better the understand the role of increased oxygen content in promoting the vanadium redox couple reaction in E-GF electrode, we carried out spin-polarized density functional theory calculations using Vienna Ab initio Simulation Package (VASP). In the simulation, the E-GF electrode was designated as —OH-terminated graphene since the exfoliation introduces hydroxyl groups (—OH) at the edge sites that contribute to most of the oxygen content in the obtained E-GF electrode, which is also in well accordance with the XPS results (Figure 4a,b). Whereas the pristine GF with low oxygen content was simulated as H-terminated graphene. The charge density differences between the two kinds of graphene are evident in Figure S13 (Supporting Information). The additional surface oxygen groups in —OH-terminated graphene created localized states around the —OH dopant when there was an extra +1/−1 charge, which was transferred from VO_2^+/VO^{2+} and V^{2+}/V^{3+} to E-GF electrodes. This suggests an increase in charge concentration in the system for the E-GF electrode compared to the pristine GF electrode. Therefore, it is apparent that the increased oxygen content in the E-GF electrode facilitates electron transport in VO_2^+/VO^{2+} and V^{2+}/V^{3+} redox couple reaction by increasing the local charge concentration in the system, which further enhances the electrochemical performance of the E-GF electrode.

3. Conclusion

In summary, we investigated the impact of the hierarchical core–shell fiber framework enriched with functional oxygen groups on the E-GF electrode in promoting the redox reaction of VRFB. Core–shell fiber framework with increased hydrophilicity, enhanced mass transfer, and abundant reaction sites for the redox couple was created by electrochemical exfoliation of GF in aqueous $(NH_4)_2SO_4$ solution. We studied different exfoliation time and various electrolyte solutions, and revealed that the electrode exfoliated for one min in 0.1 M $(NH_4)_2SO_4$ aqueous solution shows the optimal redox onset potentials, lowest ΔE, and highest $-I_{Pc}/I_{Pa}$ ratio in this work (The treatment condition might change with different carbon electrode). The as-prepared E-GF electrode exhibits an increase in the specific surface area as verified by the BET results and a substantial enhancement in electrochemical performance in the VRFB, confirming the beneficial role of functional oxygen groups incorporated in

the GF electrode. Consequently, the E-GF electrode obtains a volumetric capacity of ≈23.94 A h L^{-1}. Further, the E-GF electrode regains ≈98% of its initial capacity when returned to the initial current density of 40 mA cm^{-2}, suggesting an excellent rate performance. In addition, E-GF electrode achieves a VE of 89.72%, EE of 86.41% at 100 mA cm^{-2}, which verifies superior mass and charge transfer of the E-GF electrode in the VRFB. Furthermore, an in-depth study using spin-polarized density functional theory further verifies a faster electron transport and reduced discharge overpotential in the as-prepared E-GF electrode. In addition to offering significant improvements in the performance of the VRFB, the approach of room temperature, one min electrochemical exfoliation in low cost and friendly aqueous solution to modify GF electrodes holds great promise for large scale industrial application as the process is rapid, scalable, and energy efficient. This investigation will open a new avenue of an effective and promising graphite electrode surface modification for various applications.

4. Experimental Section

Treatment of Electrodes: AvCarb G100 Soft Graphite Battery Felt (Fuel cell store, USA) was used for the entire work. The electrochemical exfoliation was conducted in a two-electrode setup, where the pristine GF was used as both cathode and anode, and a 0.1 M $(NH_4)_2SO_4$ (Fisher Scientific, USA) aqueous solution was used as the electrolyte. In addition, various other electrolytes including 0.1 M $(NH_4)_2SO_4$ with TEMPO (Sigma-Aldrich, USA), 0.1 M $(NH_4)_2SO_4$ with 10% ethanol (Fisher Scientific, USA), 0.1 M $(NH_4)_2SO_4$ with 0.1 M sodium hydroxide (NaOH) (Fisher Scientific, USA), and 0.1 M sulfuric acid (H_2SO_4) (Sigma-Aldrich, USA) were also tested as electrolytes. The distance between the two electrodes was kept constant at ≈2 cm throughout the electrochemical process. A positive bias voltage of 10 V was applied for various times starting from 30 s to 4 min on both sides of the GF and the felts were washed several times with deionized water to get rid of any residual electrolyte. To prepare the T-GF electrodes, the pristine GF were thermally treated in a tube furnace in an air atmosphere at 400 °C for 10 h. The A-GF electrodes were obtained by treating the pristine GF with a concentrated 3:1 mixture of sulfuric acid and nitric acid at 60 °C for 6 h. All the samples were thoroughly washed and sonicated in deionized water for 5 min before use.

Characterization: CV experiments were performed using a Biologic SP150 potentiostat controlled by Biologic EC-Lab software. A graphite rod and Ag/AgCl were used as the counter and reference electrodes, respectively. The working electrodes were prepared by attaching a piece of carbon felt at the tip of a graphite rod to ensure a similar surface area for all the electrodes, and a 0.1 M vanadyl sulfate ($VOSO_4$) (Sigma-Aldrich, USA) solution was used as the electrolyte for all the CV experiments. Note that the second cycle of the CV was used for all the samples. In addition, the morphology of the pristine GF and E-GF was characterized by an FE-SEM (SUPRA 25, USA) using an accelerating voltage of 5 K eV. The structure of the samples was characterized by Raman spectra (Lab Ram HR800 UV NIR with 532 nm laser excitation) and X-ray diffraction (PANalytical/Philips X'Pert Pro scattering system with Ni-filtered Cu Kα radiation). The surface composition of the GF samples was analyzed using XPS (Thermo Scientific K-Alpha). The specific surface area was determined by Brunauer–Emmett–Teller (Micromeritics 3 Flex surface characterization tool) using nitrogen adsorption–desorption.

Flow Cell Test: The setup of the flow cell was described in detail in a previous work.[45] The active area of the electrodes on both sides is 5 cm^2, and the cell was assembled using a Nafion 115 membrane (Chemours, USA). The membranes were pretreated by boiling at 85 °C in deionized water for 15 min followed by soaking in 5% H_2O_2 solution for 30 min. Afterward, the membranes were rinsed thoroughly with deionized water and soaked in 0.1 M H_2SO_4 solution for 30 min and washed with deionized water before use. The cell also contained two electrolyte reservoirs of 50 mL. The electrolytes were pumped at a flow rate of 20 mL min^{-1} using a peristaltic pump and the flow rate was kept constant for all the experiments. The positive and negative sides were sparged with nitrogen gas before running and sealed properly to prevent oxygen exposure. Initially, the electrolytes were prepared by dissolving 1 M $VOSO_4$ in 3 M H_2SO_4 solution. To prepare the positive and negative side electrolytes, the cell was charged at a constant voltage of 1.75 V until the current dropped below 5 mA, which is an indication of complete conversion to V(V) and V(II) on the positive and negative sides, respectively.

EIS was performed at open circuit potential by applying a sinusoidal voltage waveform of amplitude 10 mV added to an offset voltage. The frequency of the sinusoidal voltage was varied stepwise from 100 kHz to 100 mHz, with six points per decade in logarithmic spacing. The electrochemical charge–discharge of the flow cell was conducted using a potentiostat (LAND, China) under a constant current density ranging from 40 to 200 mA cm^{-2}.

Computational Details: Spin-polarized density functional theory calculations were performed using VASP[46] with projector augmented wave (PAW) pseudopotential[47] and Perdew–Burke–Ernzerhof (PBE) exchange-correlation functional.[48] A kinetic energy cutoff of 400 eV was adopted for the plane-wave expansion, and all atomic positions were fully relaxed until the final force on each atom was less than 0.05 eV $Å^{-1}$.

Supporting Information

Supporting Information is available from the Wiley Online Library or from the author.

Acknowledgements

A.M. and Y.Y. contributed equally to this work. This research was supported by the Tier 1 award from Northeastern University and Rogers Corporation. The authors acknowledge the Kostas Nanomanufacturing Research Center for sharing the Scanning electron microscope, X-ray diffraction, and four-point probe conductivity measurement device. The authors also extend their gratitude to the Center for Nanoscale Systems (CNS) Harvard for providing access to their X-ray photoelectron spectroscopy and Brunauer–Emmett–Teller instruments. The DFT calculations are supported by Welch Foundation (Grant No. F-1959-20180324) and the startup grant from The University of Texas at Austin (UT Austin), and used computational resources located at the National Renewable Energy Laboratory (NREL) sponsored by the DOE's Office of Energy Efficiency and Renewable Energy (EERE), and used the Texas Advanced Computing Center (TACC) at UT Austin.

Conflict of Interest

The authors declare no conflict of interest.

Keywords

electrochemical exfoliation, hydrophilicity, kinetic, redox flow battery, surface treatment

Received: April 19, 2019
Revised: June 25, 2019
Published online:

[1] Y. Liu, Y. Shen, L. Yu, L. Liu, F. Liang, X. Qiu, J. Xi, *Nano Energy* **2018**, *43*, 55.
[2] B. Li, M. Gu, Z. Nie, Y. Shao, Q. Luo, X. Wei, X. Li, J. Xiao, C. Wang, V. Sprenkle, *Nano Lett.* **2013**, *13*, 1330.
[3] Q. Deng, P. Huang, W. X. Zhou, Q. Ma, N. Zhou, H. Xie, W. Ling, C. J. Zhou, Y. X. Yin, X. W. Wu, *Adv. Energy Mater.* **2017**, *7*, 1700461.
[4] K. J. Kim, M.-S. Park, Y.-J. Kim, J. H. Kim, S. X. Dou, M. Skyllas-Kazacos, *J. Mater. Chem. A* **2015**, *3*, 16913.
[5] B. Sun, M. Skyllas-Kazakos, *Electrochim. Acta* **1991**, *36*, 513.
[6] M. A. Aziz, S. Shanmugam, *J. Power Sources* **2017**, *337*, 36.
[7] A. Di Blasi, C. Busaccaa, O. Di Blasia, N. Briguglioa, G. Squadritoa, V. Antonuccia, *Appl. Energy* **2017**, *190*, 165.
[8] M. G. Hosseini, S. Mousavihashemi, S. Murcia-López, C. Flox, T. Andreu, J. R. Morante, *Carbon* **2018**, *136*, 444.
[9] J. Vázquez-Galván, C. Flox, C. Fàbrega, E. Ventosa, A. Parra, T. Andreu, J. R. Morante, *ChemSusChem* **2017**, *10*, 2089.
[10] M. Jing, X. Zhang, X. Fan, L. Zhao, J. Liu, C. Yan, *Electrochim. Acta* **2016**, *215*, 57.
[11] X. Wu, H. Xu, L. Lu, H. Zhao, J. Fu, Y. Shen, P. Xu, Y. Dong, *J. Power Sources* **2014**, *250*, 274.
[12] A. W. Bayeh, D. M. Kabtamu, Y.-C. Chang, G.-C. Chen, H.-Y. Chen, G.-Y. Lin, T.-R. Liu, T. H. Wondimu, K.-C. Wang, C.-H. Wang, *ACS Sustainable Chem. Eng.* **2018**, *6*, 3019.
[13] A. Fetyan, G. A. El-Nagar, I. Derr, P. Kubella, H. Dau, C. Roth, *Electrochim. Acta* **2018**, *268*, 59.
[14] B. Li, M. Gu, Z. Nie, X. Wei, C. Wang, V. Sprenkle, W. Wang, *Nano Lett.* **2014**, *14*, 158.
[15] Z. González, C. Flox, C. Blanco, M. Granda, J. R. Morante, R. Menéndez, R. Santamaría, *J. Power Sources* **2017**, *338*, 155.
[16] P. Han, H. Wang, Z. Liu, X. Chen, W. Ma, J. Yao, Y. Zhu, G. Cui, *Carbon* **2011**, *49*, 693.
[17] W. Li, J. Liu, C. Yan, *Electrochim. Acta* **2012**, *79*, 102.
[18] W. Li, J. Liu, C. Yan, *Carbon* **2011**, *49*, 3463.
[19] S. Wang, X. Zhao, T. Cochell, A. Manthiram, *J. Phys. Chem. Lett.* **2012**, *3*, 2164.
[20] P. Huang, W. Ling, H. Sheng, Y. Zhou, X. Wu, X.-X. Zeng, X. Wu, Y.-G. Guo, *J. Mater. Chem. A* **2018**, *6*, 41.
[21] H. R. Jiang, W. Shyy, L. Zeng, R. H. Zhang, T. S. Zhao, *J. Mater. Chem. A* **2018**, *6*, 13244.
[22] B. Sun, M. Skyllas-Kazacos, *Electrochim. Acta* **1992**, *37*, 1253.
[23] Z. Zhang, J. Xi, H. Zhou, X. Qiu, *Electrochim. Acta* **2016**, *218*, 15.
[24] J. J. Park, J. H. Park, O. O. Park, J. H. Yang, *Carbon* **2016**, *110*, 17.
[25] K. Parvez, R. Li, S. R. Puniredd, Y. Hernandez, F. Hinkel, S. Wang, X. Feng, K. Müllen, *ACS Nano* **2013**, *7*, 3598.
[26] J. Lu, J.-X. Yang, J. Wang, A. Lim, S. Wang, K. P. Loh, *ACS Nano* **2009**, *3*, 2367.
[27] K. Parvez, Z.-S. Wu, R. Li, X. Liu, R. Graf, X. Feng, K. Müllen, *J. Am. Chem. Soc.* **2014**, *136*, 6083.
[28] L. Wu, Y. Shen, L. Yu, J. Xi, X. Qiu, *Nano Energy* **2016**, *28*, 19.
[29] P. K. Sonkar, K. Prakash, M. Yadav, V. Ganesan, M. Sankar, R. Gupta, D. K. Yadav, *J. Mater. Chem. A* **2017**, *5*, 6263.
[30] R. Sadri, M. Hosseini, S. Kazi, S. Bagheri, N. Zubir, K. Solangi, T. Zaharinie, A. Badarudin, *J. Colloid Interface Sci.* **2017**, *504*, 115.
[31] G. Wu, B.-Q. Xu, *J. Power Sources* **2007**, *174*, 148.
[32] D. M. Kabtamu, J.-Y. Chen, Y.-C. Chang, C.-H. Wang, *J. Power Sources* **2017**, *341*, 270.
[33] L. Cao, M. Skyllas-Kazacos, D.-W. Wang, *J. Electrochem. Soc.* **2016**, *163*, A1164.
[34] T. Liu, X. Li, H. Nie, C. Xu, H. Zhang, *J. Power Sources* **2015**, *286*, 73.
[35] L. Zhang, Z.-G. Shao, X. Wang, H. Yu, S. Liu, B. Yi, *J. Power Sources* **2013**, *242*, 15.
[36] K. J. Kim, S.-W. Lee, T. Yim, J.-G. Kim, J. W. Choi, J. H. Kim, M.-S. Park, Y.-J. Kim, *Sci. Rep.* **2015**, *4*, 6906.
[37] J. Noack, N. Roznyatovskaya, J. Kunzendorf, M. Skyllas-Kazacos, C. Menictas, J. Tübke, *J. Energy Chem.* **2018**, *27*, 1341.
[38] H. Fink, J. Friedl, U. Stimming, *J. Phys. Chem. C* **2016**, *120*, 15893.
[39] A. Bourke, M. Miller, R. P. Lynch, X. Gao, J. Landon, J. Wainright, R. Savinell, D. Buckley, *J. Electrochem. Soc.* **2016**, *163*, A5097.
[40] L. Shi, S. Liu, Z. He, H. Yuan, J. Shen, *Electrochim. Acta* **2015**, *178*, 748.
[41] J. Jin, X. Fu, Q. Liu, Y. Liu, Z. Wei, K. Niu, J. Zhang, *ACS Nano* **2013**, *7*, 4764.
[42] D. Aaron, Z. Tang, A. B. Papandrew, T. A. Zawodzinski, *J. Appl. Electrochem.* **2011**, *41*, 1175.
[43] H. Zhang, H. Zhang, F. Zhang, X. Li, Y. Li, I. Vankelecom, *Energy Environ. Sci.* **2013**, *6*, 776.
[44] J. S. Lawton, A. Jones, T. Zawodzinski, *J. Electrochem. Soc.* **2013**, *160*, A697.
[45] A. Mukhopadhyay, J. Hamel, R. Katahira, H. Zhu, *ACS Sustainable Chem. Eng.* **2018**.
[46] a) P. Lehtinen, A. S. Foster, A. Ayuela, A. Krasheninnikov, K. Nordlund, R. M. Nieminen, *Phys. Rev. Lett.* **2003**, *91*, 017202; b) A. Krasheninnikov, P. Lehtinen, A. S. Foster, P. Pyykkö, R. M. Nieminen, *Phys. Rev. Lett.* **2009**, *102*, 126807.
[47] a) G. Kresse, D. Joubert, *Phys. Rev. B* **1999**, *59*, 1758; b) P. E. Blöchl, *Phys. Rev. B* **1994**, *50*, 17953.
[48] a) G. Kresse, J. Furthmüller, *Phys. Rev. B* **1996**, *54*, 11169; b) J. P. Perdew, K. Burke, M. Ernzerhof, *Phys. Rev. Lett.* **1996**, *77*, 3865.